Flowfield Interactions Induced by Massive Lateral Injection

H. Rosenbaum,* D. Siegelman,† and R. C. Boger‡
Avco Systems Division, Wilmington, Mass.

Experiments have been conducted on a slender cone at Mach 20 with massive discrete injection to determine the flowfield interaction, including boundary-layer separation and its influence upon aerodynamic coefficients. It was found that the massive injection rates caused the boundary layer to separate to the cone nose, yielding a separation shock system symmetric with respect to the wind vector. This separation system, which engulfs the conical body, remains fixed with respect to the wind vector while the conical body follows its angle of attack oscillation within it. The resulting body forces and moments are statically stabilizing. The experiments suggest a straightforward analytical model to describe the jet/flowfield interaction and resultant boundary-layer separation. This model is used to compute the pressures, forces, and moments acting on the body. The analytical results compare well with the experiments. The transverse jet hypersonic flow interaction resulted in large unsteady oscillations. High-speed optical and high-frequency pressure diagnostics were used to frequency analyze the oscillations, which bear a marked resemblance to those occurring in hypersonic flow over spiked bodies.

I. Introduction

A SERIES of experiments has been conducted to study the hypersonic flowfield interaction induced by highly underexpanded jets located on the periphery of a slender cone and exhausting normal to the body surface. The test results include surface pressure, six degree-of-freedom aerodynamic forces and moments, and schlieren still and movie coverage.

It was recognized in previous work[1] that large areas of separated flow could be induced on a body with massive injection. The flow separation in turn can cause static instabilities and result in nonzero stable static trim angles. In the present series of tests, injection for the most part was so massive that laminar boundary-layer separation extended to the cone nose, even at angle of attack. The result of this is to lead to a configuration which is at least statically stable. In fact, it will be shown that for most cases, stability increases.

These experiments have led to a straightforward analysis of the hypersonic interaction between the injectant and freestream. It is observed that the separation shock system remains symmetric to the freestream as the conical body undergoes angle of attack oscillation. Jet penetration heights on both windward and leeward sides are shown to adjust by means of a secondary shock system to accommodate the symmetric separation system. Surface pressures and aerodynamic coefficients are then modeled as a function of angle of attack and roll rate. Comparison with the measured values is acceptable.

II. Description of Experiment

The tests were conducted in Tunnel F of the von Karman Gas Dynamics Facility at AEDC. This arc-driven hypervelocity wind tunnel is capable of Mach 20 flow in the 108-in. diam test section and Reynolds numbers between 0.04×10^6 and 1.0×10^6 ft. These conditions allow simulation of the flight Mach number and Reynolds number environment between 125,000- and 200,000-ft altitude. Interest is in the upper range of this altitude band, where plume interactions are very pronounced and laminar separated flow is expected. The mass flux rates to be used have been chosen on the basis of a previous series of tests.[2] On this basis, two mass injection rates, which result in interaction shocks extending to 3 and 4 times the model's base radius, have been chosen.

The model was a 6° half-angle cone with a 4-in. base diameter (Fig. 1). Four sonic orifices were located 90° apart on the cone surface 2 in. forward of the base. The tests were divided into two series. The first was a force entry to determine the six components of forces and moments acting upon the body. Mass flow rate, Reynolds number, model angle of attack, and roll angle were varied during the test. The second series of tests involved the use of a pressure instrumented model. The same parameters were varied, with the principal test objective being the determination of separation patterns and pressures. The model and force balance assembly were supported on a sting, which also served as the gas supply pipe. Both high-speed and still schlieren photography were used to aid in test diagnostics.

The force model used was turned from balsa concentric with the balance axis. An aluminum tip was fitted to the balsa and a magnesium skirt was bonded inside the balsa skirt for added strength in the vicinity of the nozzles and plenum. The balsa was sealed and finished with a hard plastic coating. The model weight was approximately 200 gm.

The pressure model consisted of an aluminum shell attached to the same plenum and sting used in the force tests. It was identical in external dimensions with the force test model. Fifty-four pressure gages were arrayed over the surface and base of the cone as follows. On the meridians $\varphi=0°$, 90°, and 180°, 13 gages were situated 1 in. apart, starting upstream of the nozzles. On the meridians $\varphi=45°$ and 135°, 6 gages were situated every 2 in. forward of the nozzles. The size of the pressure gages limited the instrumentation of the tip. Three taps were located on the base at $\varphi=0°$, 90°, and 180°.

The mass injection system consisted of a 475-in.[3] nitrogen storage tank equipped with external resistance heaters and a fast-response explosive-driven valve capable of opening in 3 msec. A complete description of the model installation and

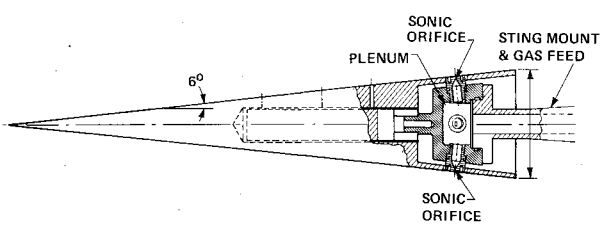

Fig. 1 Schematic of model.

Received November 13, 1974; revision received March 31, 1975.
Index categories: Jets, Wakes, and Viscid-Inviscid Flow Interactions; Entry Vehicle Dynamics and Control; Supersonic and Hypersonic Flow.

*Senior Consulting Scientist. Member AIAA.

†Group Leader. Member AIAA.

‡Senior Staff Scientist. Now with DuPont Research Laboratories. Associate Member AIAA.

the extensive calibration is given in Ref. 3. Tables 1 and 2 show the test matrix for the force and pressure tests, respectively.

III. Results of the Experiment

Figure 2 shows some representative schlieren photographs of the hypersonic interaction. The Reynolds number is about 0.3×10^6/ft and Mach number is nominally 20 for all three runs. It is immediately evident that the interaction causes the boundary layer to separate almost to the model nose. It can also be observed that the separation pattern is independent of roll and that an angle of attack the separation shock system is symmetric with respect to the wind vector. We will have more to say about these latter two observations in the modeling section.

Table 1 AEDC test summary—force test

$\dot{m}^a$ (lb/sec)	α (deg)	ϕ (deg)	$Re_{\infty,\ell}$ (10^{-6})	M_∞	Run no.
0.370	0	0	0.26	19.7	4285
0.369	0	0	0.25	18.8	4307
0.359	2	0	0.38	20.2	4301
0.351	2	0	0.30	19.4	4305
0.376	2	0	0.23	19.0	4306
0.369	4	0	0.39	20.1	4309
0.363	8	0	0.25	19.4	4310
0.360	2	−22.5	0.30	19.8	4300
0.365	4	−45.0	0.34	19.3	4311
0.378	4	−90.0	0.25	18.9	4312
0.377	8	−45.0	0.34	20.3	4313
0.159	0	0	0.31	19.7	4289
0.158	2	0	0.34	20.0	4287
0.149	4	0	0.29	19.7	4286
0.105	0	0	0.40	20.4	4292
0.097	2	0	0.31	20.2	4290
0.098	2	0	0.31	19.6	4297
0.085	3	0	0.30	18.9	4302
0.104	4	0	0.33	19.5	4291
0.027	0	0	0.11	19.1	4296
0.019	2	0	0.09	19.9	4294
0.027	4	0	0.11	20.0	4295

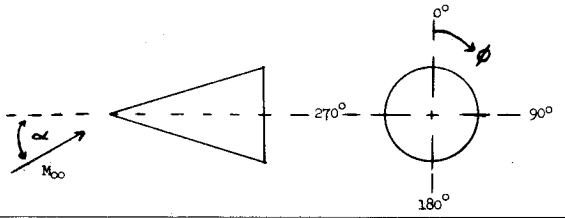

[a] $\dot{m}$ = Total mass flow from all 4 jets.

Table 2 Test summary—pressure test

$\dot{m}$ (lb/sec)	α (deg)	ϕ (deg)	$Re_{\infty,\ell}$ (10^{-6})	M_∞	Run no.
0.35	0	0	0.41	19.9	4314
0.35	2	0	0.26	20.1	4315
0.37	4	0	0.32	20.6	4316
0.37	4	+22.5	0.25	19.5	4318
0.36	4	+45.0	0.27	19.6	4317
0.16	0	0	0.30	20.3	4322
0.15	2	0	0.30	19.7	4321
0.15	4	0	0.40	20.0	4320
0.10	0	0	0.31	20.5	4323
0.10	2	0	0.33	19.7	4324
0.10	4	0	0.35	20.6	4325
0	4	0	0.30	19.9	4319

In the case of zero angle of attack, it has been shown in Ref. 2 that the penetration depth is well correlated by the model of Zukowski and Spaid.[4] This is shown in Fig. 3, where the dimensionless penetration height h/R_b, where h is the distance from the cone surface to the jet boundary and R_b is the cone base radius, is plotted vs the dimensionless mass flow per jet, $\bar{m}$. $\bar{m}$ is defined as

$$\bar{m} = (\dot{m}/4\rho_\infty U_\infty A_b)$$

where $A_b = \pi R_b^2$. The solid line is the theory of Ref. 4, which for $(\rho_\infty/\rho_{oj})^{(\gamma_j-1)/\gamma_j} << 1$ reduces to

$$h/R_b = 2\left[\frac{\gamma_j \bar{m}}{U_\infty}\right]^{1/2}\left[\frac{2R\,T_{oj}}{W_j\gamma_j(\gamma_j-1)}\right]^{1/4} \qquad (1)$$

where W_j = jet molecular weight.

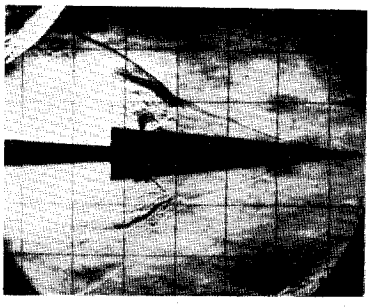

RUN 4285 $\alpha = 0$ $\varphi = 0$

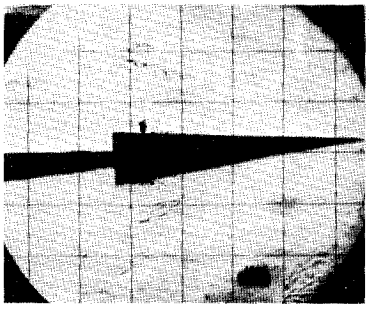

RUN 4309 $\alpha = 4$ $\varphi = 0$

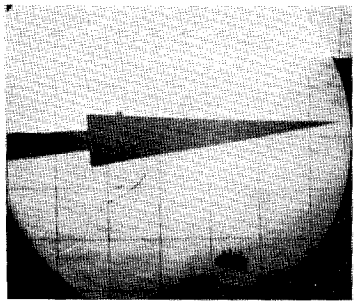

RUN 4317 $\alpha = 4$; $\varphi = 45$

Fig. 2 Schlieren photographs of the interaction flowfield.

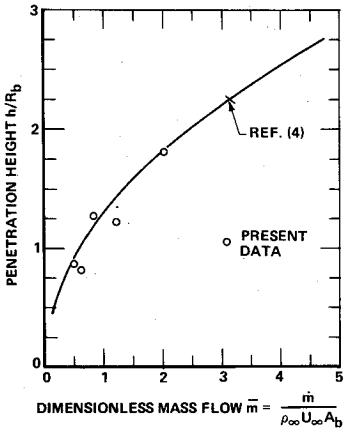

Fig. 3 Penetration height vs mass flow.

Table 2 summarizes the AEDC-VKF pressure entry test conditions. The tests were conducted at a nominal Mach number of 20 and a nominal Reynolds number of 0.3×10^6 based on model length. Mass injection rates were varied from 0 to 0.37 lb/sec. The angle of attack was varied from 0° up to 4°. There were two tests in which the model was rolled by 22.5° and 45°, respectively. The nature of the pressure distribution induced by lateral jet injection is discussed in great detail in Refs. 4-8. Typically, there is a laminar-free interaction at the separation point which results in a rapid rise from undisturbed pressure levels. This rise is followed by a region of essentially constant "plateau" pressure. A second rise in pressure exists just upstream of the injection port due to shear layer reattachment. This is followed by a rapid drop in pressure across the jet to a fairly low and constant "base pressure" level. Downstream reattachment again causes a rise in pressure, followed by a slow decay.

Some representative detailed pressure distributions are presented in Figs. 4-6. At each time point where data were taken, the axial pressure variation along a given meridian is presented. The leeside is designated "0° ray," while the windward side is the "180° ray." The injection ports are located at 0°, 90°, and 180°. As indicated, the flagged symbols present the undisturbed surface pressure distributions prior to the start of mass addition.

Several features are apparent from these figures. First, one may discern the effects of angle of attack upon the undisturbed pressure distributions. Figure 4 shows that at zero incidence the pressure levels are about 11 times ambient on all meridians. As expected from viscous interaction theory, a very slight decay in the axial direction is noted. At incidence, the windward pressure level increases significantly, while the leeside level drops slightly. This is seen in Fig. 5, where windward pressures average about 25 times ambient, while leesides are down to about 7-8 times ambient levels.

With mass injection on (unflagged symbols), the distributions tend to exhibit the classical shapes (rapid rise at separation, plateau, peak, and dropoff). Pressures downstream of the jets are at undisturbed levels or below. No second reattachment point rise is evident. This seems consistent with previous findings that at least two penetration heights must be available downstream of the jets for reattachment to occur. Elevated pressure levels are noticed well up on the nose at the highest injection rates.

The most important feature of the pressure data is the circumferential pressure variation. From Figs. 4 and 5 it is noted that plateau pressure levels on all meridians vary from about 80-90 times ambient levels over the angle attack range of 0-4°. Figure 6 indicates that this plateau level is unaffected by rolling the model. This independence of angle of attack or roll angle implies that the jet interaction produces a separation geometry which is symmetric with respect to the wind vector. This is the same conclusion reached from the schlieren data. Furthermore, it appears that the mass injection rate is the main parameter in determining the pressure levels and hence the separation geometry.

Table 1 summarizes the AEDC-VKF force entry test conditions. All tests were conducted at a nominal Mach number of 20. Most of the tests were conducted at a Reynolds number of 0.3×10^6 based on model length. Three tests were run at a Reynolds number of 0.1×10^6. Mass injection rates ranged

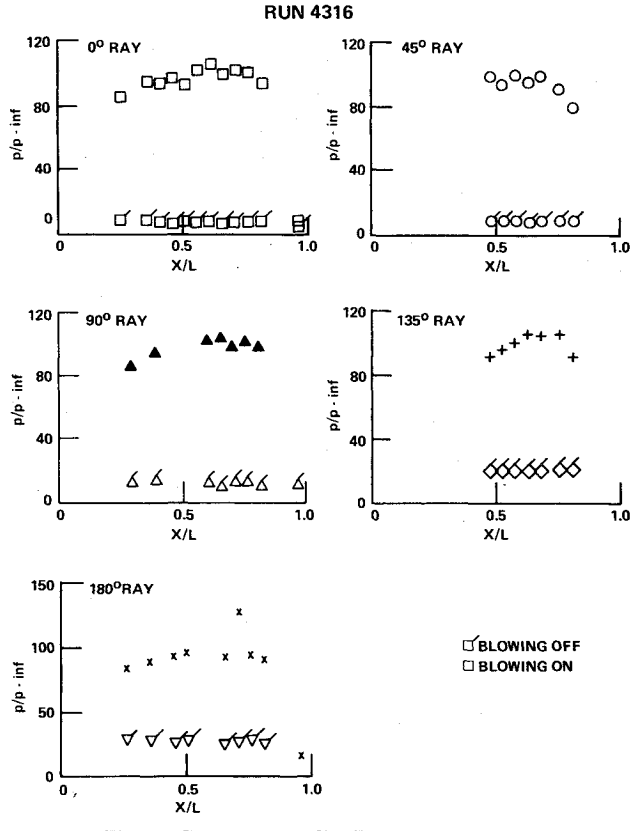

Fig. 5 Cone pressure distributions $\alpha = 4$; $\varphi = 0$.

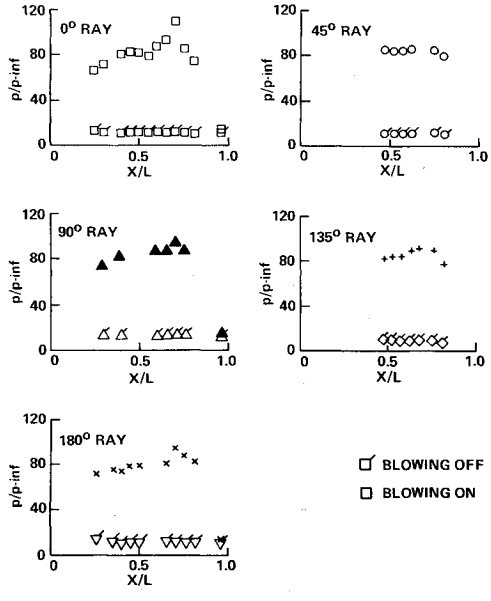

Fig. 4 Cone pressure distributions $\alpha = 0$; $\varphi = 0$.

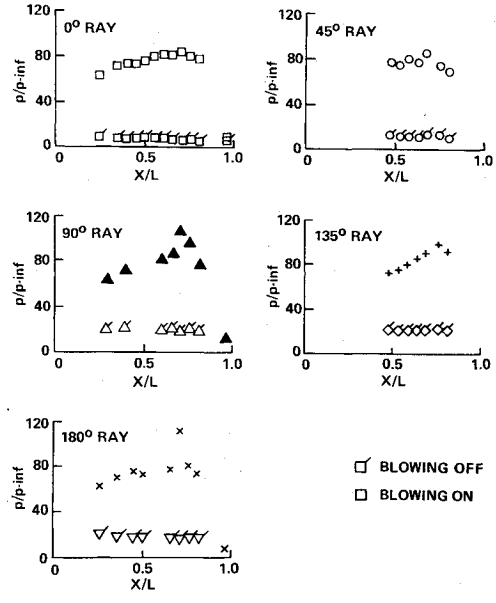

Fig. 6 Cone pressure distributions $\alpha = 4$; $\varphi = 45$.

from 0 to 0.38 lb/sec. Angles of attack up to 8° were investigated. Four tests were conducted to explore the effects of model roll angle. Roll angles of -22.5°, -45°, and -90° were studied.

Figures 7 and 8 present the results of the force entry tests. Figure 7 shows the variation of the forebody axial force coefficient with total angle of attack at high rates of mass addition. This coefficient is defined as the force on the cone frustum divided by $q_\infty A_b$. Since base contributions are small this is, in effect, the total axial force coefficient. It is clear that the effect of mass addition is to raise the axial force coefficient to a constant value of about 0.25 independent of angle of attack. This result is quite consistent with previous conclusions in that a) the jet interaction leads to higher surface pressures, which then imply increased axial force, and b) the separation geometry is insensitive to angle of attack. Figure 7b shows that the normal force coefficient (normal force/$q_\infty A_b$) has been reduced by the use of massive lateral injection. Again, this is consistent with the finding that the jet interaction results in a flowfield which is symmetric with respect to the wind vector. Thus, while it is true that overpressure levels have increased due to injection, relative differences in pressure level around the body have been reduced. The body can then oscillate freely in the constant-pressure environment provided by the interaction flowfield.

Figure 7c demonstrates the rearward motion of the center of pressure due to massive lateral injection. This migration can be understood in terms of the pressure distributions previously presented. Upstream of the injection points there is a tendency toward uniform pressures. This means that the main contributions toward the normal force and moment come from the vicinity of the jets and farther back. This then shifts the center of pressure rearward from the undisturbed location. Figures 8a and 8b show that the restoring moment has been increased due to injection. This implies that static stability has been increased.

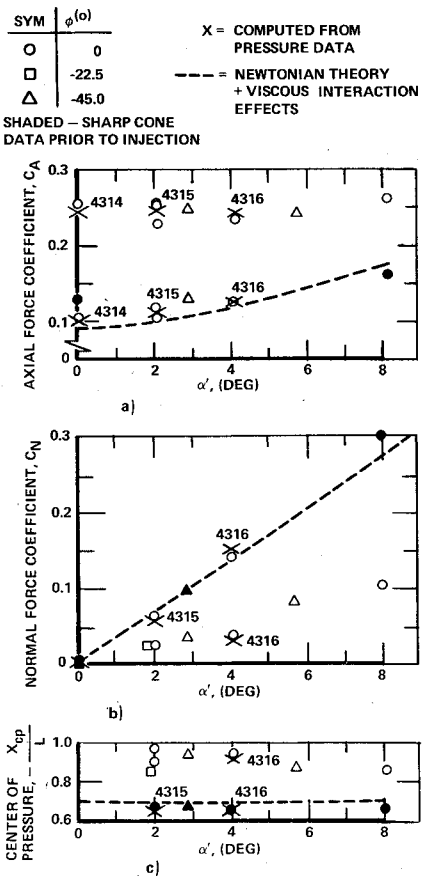

Fig. 7 a)Axial force coefficient; b) Normal force coefficient; c) Center of pressure.

IV. Aerodynamic Coefficients

The pressure distribution was integrated to obtain the aerodynamic coefficients. These are then compared with the force data to insure compatibility, give confidence in the force test procedure, and verify the assumptions concerning the pressure distribution and base pressure effects. The technique employed follows very closely that used in Ref. 1. Briefly, restricting attention to the unrolled cases, symmetry about the pitch plane was assumed and the circumferential pressure distribution was fitted to a cosine series

$$\frac{P}{P_\infty}(\bar{X}_i) = \bar{P}(\bar{X}_i) = \sum_{N=0}^{4} \bar{P}_N(\bar{X}_i)\cos^N\varphi$$

where $\bar{X}_i = X_i/L$, L = vehicle length (19.625 in.), and X_i = axial station of ith data point. The force and moment coefficients can now be calculated by appropriately integrating the aforementioned pressure distribution. It should be noted that contributions from the base are small and were neglected in the force integrals.

To complete the calculation of the aerodynamic coefficients, it is necessary to supplement some of the pressure distribution data. In particular, in the region upstream of the first pressure port and in the region between the injection ports and the base, data are particularly sparse. In the upstream region, that portion forward of separation is described by the pressure appropriate to a sharp cone plus a viscous interaction correction.[11] In the vicinity of the separation point there is a transition zone where the pressure rises from the undisturbed values to the plateau level. The axial extent of this transition zone can be estimated from the work of Lewis, Kubota, and Lees.[9] An appropriate third-order pressure distribution function was chosen to represent the pressure in the transition region.

In regard to the downstream region in the vicinity of the injection ports and beyond, it is also necessary to fill in data. In filling in the pressure distribution in the vicinity of the jets and beyond, use was made of the profile data presented in Ref. 12. This reference shows that immediately downstream of the jet, a constant rather low "base-like" pressure level exists for a distance of about 2 penetration heights. This is followed by a recompression zone, due to reattachment with a peak pressure occurring at about 6 penetration heights behind the jet port.

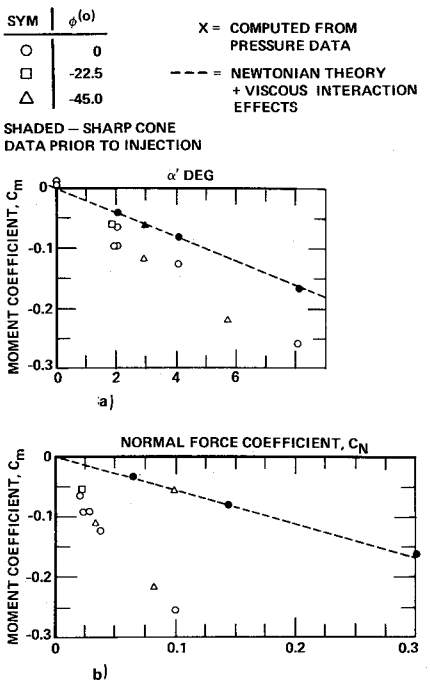

Fig. 8 a)Moment coefficient; b) Moment vs normal force.

For the configuration of present concern and at the blowing rates of interest, the penetration heights were sufficiently large such that no downstream reattachment on the cone surface is likely. Thus, the one available measurement is most probably indicative of a constant "base-like" pressure zone.

With these arguments in mind it was assumed that the region from the jet to the base was at the pressure measured on the last available tap on any particular meridian of interest. Upstream of the jet, in the zone between the last available upstream data point and the jet, a cubic fit was again assumed. Comparisons of aerodynamic coefficients obtained by integration of the pressure test data with those measured in the force entry tests are shown in Figs. 7 and 8. It can be seen that excellent agreement has been achieved. This verifies the validity of both sets of data and further establishes that the force data can be understood in terms of the surface pressure distributions.

V. Interaction Flowfield

It has been seen that the effect of massive lateral injection is to produce a separation geometry which is symmetric about the wind vector even when the model is at angle of attack. The underlying physical mechanism is that the subsonic recirculating flow within the separated zone cannot support a significant pressure gradient. Thus, once the mass injection rate has increased to the point where individual jet interaction cells begin to overlap, the entire body becomes immersed in a circumferential band of subsonic flow. Since pressures within this band must be essentially constant, a geometry symmetric with respect to the wind vector must result. This tendency toward symmetry also implies that individual jets do not behave independently; that is, they are affected by the presence of the other jets and the symmetry requirement.

This is clearly evident in the schlieren photographs. The windward penetration is less than that on the leeside. Since all nozzles are of the same area and are operated at choked conditions, the mass flows are equal. One might then expect equal penetration heights, based on correlations such as those presented in Eq. (1). Equal penetrations have not resulted, however, because of the coupling which exists through the subsonic separated zones. Furthermore, the mechanism whereby such penetration height adjustments take place is through a rotation of the initial portion of the jet boundary (located just above the Mach disk). The effect of this increased rotation is to strengthen the interaction shock generated by the turning of the ambient flow to spill over the jet boundary. This produces a higher local pressure level on the jet boundary. For the static pressure behind the Mach disk to match this increased local pressure, the normal shock must occur at a reduced upstream Mach number. Thus, the penetration height is reduced.

This coupling between the invicid flow and jet boundary behavior can be clarified by consideration of the flowfield shown in Fig. 9. The shear layer separates, producing a conical dividing stream surface of half angle σ. This produces a conical separation shock of half-angle θ_σ and a corresponding conical flow with Mach number M_c and pressure $\bar{P}_c$. At the point where the shear layer attaches to the plume a second shock is generated at angle Θ_{RS}. Downstream of this shock there is a flowfield having Mach number M_2 and pressure $\bar{P}_2$. For the jet boundary line to behave as a proper slip surface this upperside pressure, $\bar{P}_2$, must equal the underside pressure, which is the static pressure behind the Mach disk, $\bar{P}_D$. The interaction shock is generated by the intersection of the separation shock and the reattachment shock. Again, a contact surface is required to separate the doubly shocked fluid from that coming across the interaction shock.

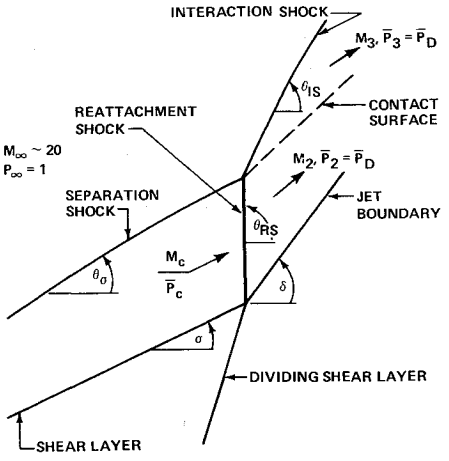

Fig. 9 Interaction flowfield model.

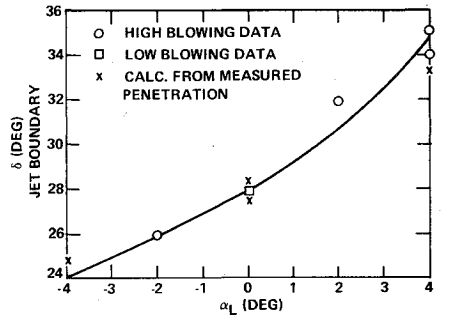

Fig. 10 Jet boundary inclination.

Calculations have been performed for windward and leeward jets at angles of attack of up to 4°. The results are shown in Fig. 10. The jet boundary inclination varies monotonically with the local incidence angle. No systematic variation with mass flow rate appears discernible. Points computed from measured jet penetration heights appear in good agreement with those measured from the photographs. Figure 11 presents the half-angle of the symmetrical conical separation surface as measured from the photographs. The plateau pressure levels were used to infer separation angles in fair agreement with those measured. Here, a systematic variation with mass flow rate is present. This is understandable in terms of available laminar separation theory.[9,10] If the expressions given in Ref. 10 are utilized and it is noted that the skin friction coefficient varies as the inverse square root of the separation Reynolds number it results that

$$(C_p)_{sep} \sim (C_{f_{sep}})^{1/2} \sim Re_{x_s}^{-1/4}$$

Now the systematic variation of the separation angle with injection rate becomes evident. As the injection rate is reduced, the penetration height decreases. Separation moves back toward the jets. The separation pressure rise is reduced and hence a smaller separation angle is implied.

It remains now to apply this model to construct the body pressure distribution analytically. This distribution can be broken down into four basic segments. Upstream of separation there is a region where undisturbed pressures exist. In the region immediately behind the separation point there is

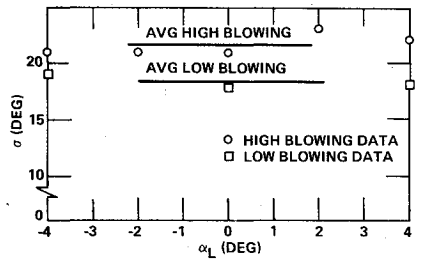

Fig. 11 Separation angle (W.R.T. wind direction).

the plateau pressure region. In this region pressures are essentially constant in both the axial and circumferential directions. Next comes the reattachment pressure spike just upstream of the jets. Lastly, there is an axially uniform region from the jets to the base.

Consider first the region behind the jets. It has been established that there is insufficient distance behind the jets for reattachment to occur. In this instance the pressure levels on the downstream body surface must reflect the turning of the flow from deflected Mach disk conditions back toward the wind vector direction. It results that these downstream pressure levels can be acceptably predicted by expanding the conditions behind the interaction shock back parallel to the wind vector.

Next consider the pressure spike region immediately upstream of the jets. The jump in pressure occurs because of the double-celled nature of the separated flow induced by the jet interaction. The dividing shear layer which separates the two recirculation cells reattaches to the body surface in this zone. The upstream end of this same shear layer is at the point where the conical separation surface reattaches to the jet plume. Since the flow is subsonic, it is reasonable to assume that pressure levels in this zone will not vary significantly from this separation surface-jet plume reattachment value. Reference 13 has been used to provide a correlation for the reattachment pressure in terms of the plateau pressure and the eventual asymptotic pressure after reattachment, which is taken to be the Mach disk value.

Since contributions to the forces and moments from the region upstream of separation are negligible, due to the relatively small surface area and pressure levels involved, only the plateau region remains to be considered. Pressure levels in this zone are governed by the symmetric separation geometry resulting from the jet interaction. It has been noted that the separation angle and resultant plateau pressure level are functions of the mass injection rate only. This has been understood in terms of the movement of the separation point with injection rate and the corresponding effect on the separation pressure rise.

Attempts to describe the measured plateau pressure data in terms of available laminar separation theories,[1,9,10,14] were not successful. All the predictions fell below the data by 25% or more. These discrepancies may be due to unsteady flow effects, apparent from the high-speed schlieren motion pictures. Alternately, these higher than expected pressures may be due to the mass venting that occurs between the jets. Since a satisfactory quantitative explanation of the plateau level was not available, the measured separation angle σ as a function of blowing parameter $\bar{m}$ was used.

The aerodynamic coefficients were calculated from the previously described pressure distribution in a manner analogous to the previous section. Figures 7 and 8 show the results of this simple interaction model, compared with the force test results and values calculated from the pressure measurements. The agreement is satisfactory.

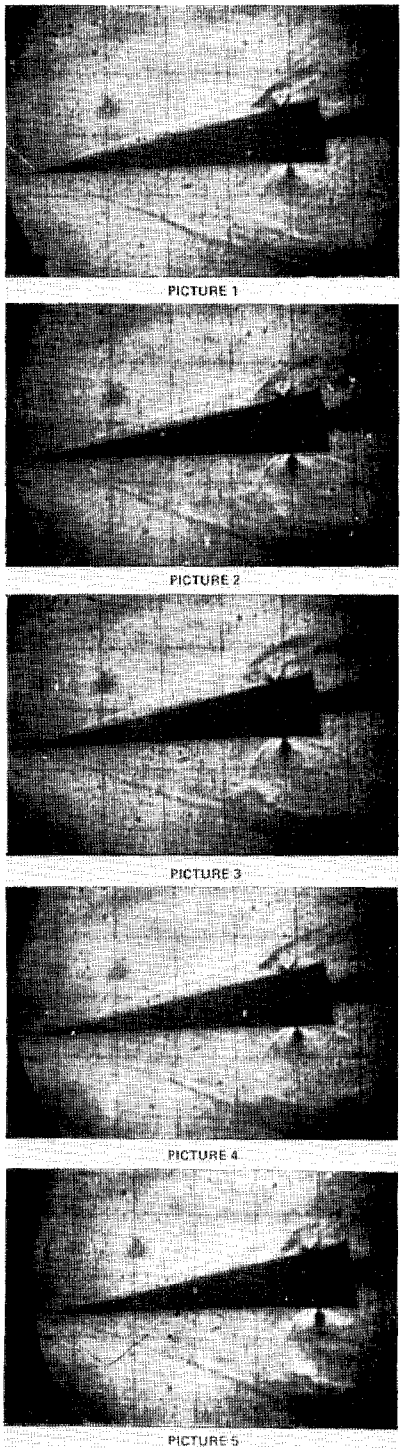

Fig. 12 Unsteady flow sequence.

VI. Unsteady Flow

It was recognized early in the test program that the interaction caused by the transverse jets resulted in rather substantial unsteady motion. This can be seen from the wavy motions of the interaction shocks (Fig. 2). An attempt was made to determine the frequency of the unsteady flow by examining the high-speed schlieren motion pictures and installing high-frequency pressure transducers on the model.

The schlieren motion pictures were taken at a framing speed of 4000 frames/sec. The quality of the motion pictures was not especially good, however, Fig. 12 shows five frames (not necessarily in order), taken from the film, which illustrate the unsteady process. The model is at a 4° angle of attack and attention is directed to the windward side. Notice that the jet penetration on the windward side goes from a minimim in picture 1 to maximum in picture 3 and back down again in picture 5. It appears that, as the jet penetration increases, the separation angle increases and the back pressure felt by the jet also increases. This then causes the jet penetration to decrease and the whole process starts over gain. It is most likely brought about by a combination of the inherent unsteady motion of the separation process, which induces a movement in the separation point along with the complex mass venting that occurs between and around the four interacting jets.

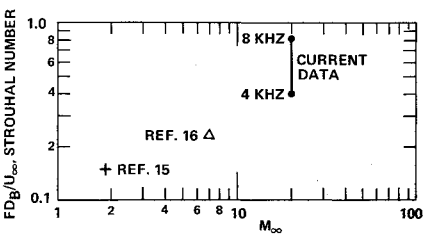

Fig. 13 Oscillation frequency.

The process has been likened to the unsteady flow over a spiked body in a supersonic stream studied by Mair,[15] Maull,[16] and others. In fact, the frequency of the oscillations noted here, when properly normalized, is in reasonably good agreement with the oscillation frequency over the spiked body. This can be seen in Fig. 13, which shows the Strouhal number vs Mach number. When the calculations of the Strouhal number were performed, the characteristic length D was taken to be the distance from the lee Mach disk to the windward Mach disk. The oscillation frequency was taken as 4000 cps, which is the maximum that could be measured by the high-speed camera.

In a further attempt to determine the character of the unsteady flow, high-frequency pressure transducers were installed in the model. The pressure transducers employed were of the semiconducter strain-gage type with a range of 0-100 psi, a sensitivity of 1.5 mv/psi, and a resonant frequency of 60 kHz. Three gages were used: one located in the separated region upstream of the injection nozzles, and the other two installed in a block near the nozzle exit. Of the two block gages, one was flush mounted and the other sealed in the block so that, by suitably combining the output of the gages, model and gage vibration could be eliminated.

Each gage was connected to separate FM channels on an Ampex portable tape deck. A total of 12 runs was recorded on tape of which 3 provided analyzable data. Spectral analysis of these three runs was performed on a Spectro Dynamics Real Times Analyzer. The analysis was performed over a frequency range of 0-16 kHz, with an effective memory of 31 msec. Since 31 msec was about the total jet on flow time, no ensembling was possible. A band-pass filter with an effective width of 200-20,000 Hz was used to remove electrical noise. It must be noted that, due to lack of real time data, accurate frequency resolution is not possible. Further, a lack of run to run repeatability, especially with the dummy gage, make run-to-run comparison difficult. With this in mind, however, the jet off, jet on data do suggest broad-band noise centered at 6 and 8 kHz, probably attributable to the jet shock interaction. Again, the frequency is in reasonable agreement with the results shown in Fig. 12. It is felt that the spectral data do not indicate the presence of boundary-layer transition.

VII. Conclusions

A series of experiments has been conducted to determine the flowfield interactions induced by massive lateral blowing on a slender cone at Mach 20. Surface pressures, forces, and moments, and still and high-speed schlieren photography were the test diagnostics. The experiment showed that the interaction caused boundary-layer separation up to the body nosetip. In fact, immediately upstream of the four lateral jets the separation patterns and hence the surface pressures were symmetric with respect to meridional planes. This pattern retained its symmetry at angle of attack resulting in a statically stable force system on the conical body.

A straight-forward analytical model was formulated with the use of the experimental observations. The interaction flowfield between the lateral jet and the freestream was modeled for zero and nonzero angles of attack. The surface pressure distribution and aerodynamic coefficients were constructed from the interaction model. The results obtained compare well with both the force and pressure test results.

Unsteady oscillations induced by jet interactions have been recognized. High-speed schlieren coverage and high-frequency pressure transducers have been used to frequency resolve the oscillations. The oscillation frequency bears a marked resemblance to that occurring in hypersonic spiked body flows.

References

[1] Boger, R. C., Rosenbaum, H., and Reeves, B. L., "Flowfield Interactions Induced by Underexpanded Exhaust Plumes," *AIAA Journal,* Vol. 10, March 1972, pp. 300-306.

[2] Reinecke, W. G., "Penetration of a Lateral Sonic Gas Jet into a Hypersonic Stream," *AIAA Journal,* Vol. 13, Feb. 1975, pp. 173-176.

[3] Siler, L. G. and Haberman, D. R., "Force and Pressure Tests on the SAMSO/Avco STREET A Vehicle with Lateral Injection at Mach 20," AEDC-TR-73-175, Oct. 1973, Arnold Engineering Development Center, Tullahoma, Tenn.

[4] Zukowski, E. and Spaid, F., "Secondary Injection of Gases into a Supersonic Flow," *AIAA Journal,* Vol. 2, Oct. 1964, pp. 1689-1696.

[5] Broadwell, J., "Analysis of the Fluid Mechanics of Secondary Injection for Thrust Vector Control," *AIAA Journal,* Vol. 1, May 1963, pp. 1067-1075.

[6] Spaid, F. W. and Zukowski, E. E., "Study of the Interaction of Gaseous Jets from Transverse Slots with Supersonic External Flows," *AIAA Journal,* Vol. 6, Feb. 1968, pp. 205-211.

[7] Hawk, N. E. and Amick, J. L., "Two-Dimensional Secondary Jet Interaction with a Supersonic Stream," *AIAA Journal,* Vol. 5, April 1967, pp. 655-659.

[8] Schetz, J. A. and Billig, F. S., "Penetration of Gaseous Jets Injected into a Supersonic Stream," *Journal of Spacecraft,* Vol. 3, Nov. 1966, pp. 1658-1665.

[9] Lewis, J. E., Kubota, T., and Lees, L., "Experimental Investigation of Supersonic Laminar, Two-Dimensional Boundary-Layer Separation in a Compression Corner with and without Cooling," *AIAA Journal,* Vol. 6, Jan. 1968, pp. 7-14.

[10] Chapman, D. R., Keuhn, D. M., and Lees, L., "Experimental Investigation of Separated Flows in Supersonic and Subsonic Streams with Emphasis on the Effect of Transition," NACA TN 3869, March 1957 (NACA Report 1356, 1958).

[11] Mirels, H. and Ellinwood, J. W., "Viscous Interaction Theory for Slender Axisymmetric Bodies in Hypersonic Flow," *AIAA Journal,* Vol. 6, Nov. 1968, pp. 2061-2070.

[12] Barnes, J. W., Davis, J. G., and Tang, H. H., "Control Effectiveness of Transverse Jets Interacting with a High-Speed Freestream," AFFDL TR-67-90, Vol. 1, Sept. 1967, Air Force Flight Dynamics Lab., Wright-Patterson Air Force Base, Ohio.

[13] Nash, J. F., "Analysis of Two-Dimensional Base Flow including the Effect of the Approaching Boundary Layer," R&M No. 3344, 1963, Aeronautical Research Council, London.

[14] Bondarev, S. N., "Boundary-Layer Separation on Conical Bodies," *Mekhanika Zhidkosti I Gaza,* Vol. 4, No. 4, pp. 46-52, 1969.

[15] Mair, W. A., "Experiments on Separation of Boundary Layers on Probes in Front of Blunt Nosed Bodies in a Supersonic Air Stream," *The Philosophical Magazine,* Vol. 43, 1952, pp. 695-714.

[16] Maull, D. J., "Hypersonic Flow over Axially Symmetric Spiked Bodies," *Journal of Fluid Mechanics,* Vol. 8, Pt. 4, 1960, pp. 584-592.